Progress In Electromagnetics Research, Vol. 132, 571–586, 2012

INTERFEROMETRIC ISAR IMAGING ON MARITIME TARGET APPLICATIONS: SIMULATION OF REALISTIC TARGETS AND DYNAMICS

D. Felguera-Martín*, J. T. González-Partida, and M. Burgos-García

Microwave and Radar Group, Department of Signals, Systems and Radiocommunications, Escuela Técnica Superior de Ingenieros de Telecomunicación, Technical University of Madrid, Madrid 28040, Spain

Abstract—ISAR imaging of maritime targets has greater success than other ISAR applications due to the constant oscillatory motions induced by waves and wind. However, relative target motions are usually unknown, difficult focusing, image interpretation and target classification. Using interferometry to obtain the height information makes possible to obtain a 3-D reconstruction of a target, aiding image focusing, image interpretation and target classification. However, the information and utility of the ISAR image and the interferometric information depends highly on geometry and targets dynamics. In this paper we will study the influence of movement dynamics in interferometric ISAR imaging using a realistic extended moving target simulation, a general geometry and complex dynamics models.

1. INTRODUCTION

Inverse Synthetic Aperture Radar (ISAR) is a technique that allows to generate range-Doppler radar images of moving targets [1]. Range resolution is guaranteed by transmitting a large signal bandwidth but cross-range resolution depends on variations of the aspect angle induced, mainly, by target dynamics. Applications of ISAR for imaging of land moving targets [2–4], airborne targets [5, 6] and space-borne targets [7] has been reported in the literature. However, ISAR imaging of maritime targets [8, 9] has greater practical success than the previous examples. This is explained due to the constant oscillatory motions,

Received 8 September 2012, Accepted 12 October 2012, Scheduled 16 October 2012

* Corresponding author: David Felguera-Martin (felguera@gmr.ssr.upm.es).

both linear and angular, that waves and wind induce in the maritime target. The nature of the relative motion defines how the target maps, by a 2-D projection, into the range-Doppler image. Moreover, if the aspect angle varies at various combinations of elevation and azimuth angles a 3-D reconstruction of the ship is even possible [10].

However, to obtain a 3-D reconstruction of the target a sufficient sampling of the 3-D Fourier space is needed, which is only obtained with very complicated and non realistic motions. In addition, a very precise knowledge of movement dynamics is needed to place each signal sample in the correct position of the Fourier space. In practice, relative target motions are usually unknown making direct 3-D imaging not feasible and even making difficult 2-D image focusing and also image interpretation.

Interferometric ISAR (InISAR) employs more than one phase centre in the radar instrument to reconstruct a 3-D target [11–13]. Typically, two vertically displaced receivers are used to retrieve the height information from the phase difference of a pair of ISAR images. Using interferometry to obtain the height information makes possible to obtain a 3-D reconstruction of a target with a simple and realistic motion and can also aid image focusing, image interpretation and target classification [14–17]. However, the information and utility of the ISAR image and the interferometric information depends highly on geometry and target dynamics.

In this paper we will study the influence of movement dynamics in interferometric ISAR imaging. For that purpose we will use a general geometry, complex motion model and a realistic extended moving target simulation, all described in Section 2. Interferometric signal processing will be described in Section 3 and some examples of the benefits of using Interferometric ISAR for maritime target imaging and image interpretation will be given in Section 4. Finally, some conclusions will be stated in Section 5.

2. MARITIME TARGET SIMULATION

In this section we will describe the general imaging geometry, the dynamics models, the extended target model and the signal models used to simulate the echo signal obtained from an extended moving target in a high resolution radar.

2.1. Imaging Geometry

The imaging geometry used in the simulations is shown in Figure 1. Radar coordinate Frame is located at O with $\hat{x}$, $\hat{y}$, $\hat{z}$ axes. Target

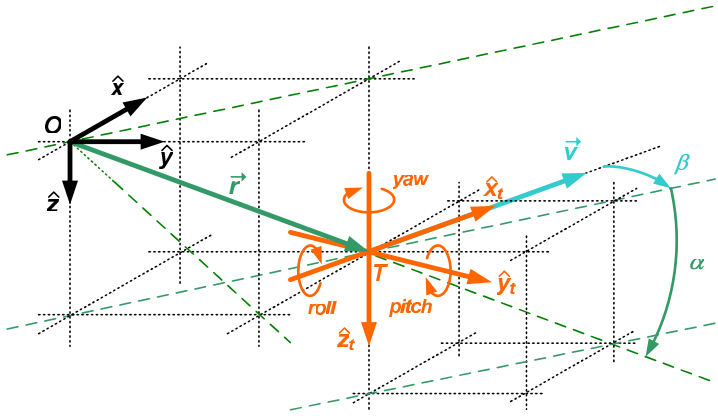

Figure 1. Imaging geometry.

coordinate Frame is located at T, which is the centre of rotation of the target, with the $\hat{x}_t$ axis along the longitudinal ship axis, the $\hat{y}_t$ axis along the transverse axis and the $\hat{z}_t$ being the cross product of previous axes. Rotation around those axes are denoted roll, pitch and yaw respectively. The distance between the radar and the target is denoted by $\vec{r}$. The direction of this vector is usually call the Line-Of-Sight (LOS). Target velocity vector is denoted by $\vec{v}$, in the absence of any rotation the $\hat{x}_t$ axis will be aligned with the velocity vector. The angle between the velocity vector and the LOS vector projected into the $\hat{r} - \hat{z}$ plane is called the gracing angle α. The angle between the velocity vector and the LOS vector projected into the $\hat{x} - \hat{y}$ plane is called the aspect angle β. When $\beta = 0°$ the target is said to be oriented in LOS direction and when $\beta = 90°$ the target is oriented in Cross-LOS direction.

2.2. Dynamics Model

The dynamics model considers the targets as a rigid-body of scattering reflectors located at coordinates $[X_0\ Y_0\ Z_0]$ respect to its centre of mass. The position of the reflectors is given by (1) and is the result of a rotation around the centre of mass due to the attitude angles, a rotation to orientate the target and a translation to the absolute position $[r_x\ r_y\ r_z]$. Attitude angles are denoted by θ_j where the suffix j represents the axis associated to the rotation. Orientation angles are the gracing angle α and the aspect angle β described before.

$$\begin{pmatrix} X \\ Y \\ Z \end{pmatrix} = R_x(\theta_x) \cdot R_y(\theta_y) \cdot R_z(\theta_z) \cdot R_z(\beta) \cdot R_y(\alpha) \cdot \begin{pmatrix} X_0 \\ Y_0 \\ Z_0 \end{pmatrix} + \begin{pmatrix} r_x \\ r_y \\ r_z \end{pmatrix} \quad (1)$$

$$R_x(\theta_x) = \begin{pmatrix} 1 & 0 & 0 \\ 0 & +\cos(\theta_x) & -\sin(\theta_x) \\ 0 & +\sin(\theta_x) & +\cos(\theta_x) \end{pmatrix} \quad (2)$$

$$R_y(\theta_y) = \begin{pmatrix} +\cos(\theta_y) & 0 & +\sin(\theta_y) \\ 0 & 1 & 0 \\ -\sin(\theta_y) & 0 & +\cos(\theta_y) \end{pmatrix} \quad (3)$$

$$R_z(\theta_z) = \begin{pmatrix} +\cos(\theta_z) & -\sin(\theta_y) & 0 \\ +\sin(\theta_z) & +\cos(\theta_z) & 0 \\ 0 & 0 & 1 \end{pmatrix} \quad (4)$$

$$R_z(\alpha) = \begin{pmatrix} +\cos(\alpha) & -\sin(\alpha) & 0 \\ +\sin(\alpha) & +\cos(\alpha) & 0 \\ 0 & 0 & 1 \end{pmatrix} \quad (5)$$

$$R_y(\beta) = \begin{pmatrix} +\cos(\beta) & 0 & +\sin(\beta) \\ 0 & 1 & 0 \\ -\sin(\beta) & 0 & +\cos(\beta) \end{pmatrix} \quad (6)$$

In order to model the translational movement a lineal, or short order, polynomial is used. For sort integrations times typically employed in ISAR imaging this is a good approximation, [6]. The model is shown in (7) where the suffix i indicates the component x, y, or z of the vector $\vec{r}$ that indicate the position of the centre of rotation of the target T.

$$r_i = r_{i_0} + \sum_{k=1}^{K} c_{i_k} \cdot t^k \quad (7)$$

For the rotational movements three models are considered. In these models the suffix i stands for *roll*, *pitch*, or *yaw* that are the angles related to the x, y, or z axes. The initial angle is represented by θ_{i_0}, the period is T_i and the maximum angle deviation is θ_{i_M}. The first model (8) is a linear model which is typical in circular paths or curve bends. The second one (9) is the sinusoidal model which is typically assumed in most papers [10]. The third model, that we propose in (9),uses a correlated Gaussian signal whose correlation time coincides with the period of the sinusoidal movement. In this model a AWGN signal with unit variance and zero mean $W_i(\omega)$ is filtered in the

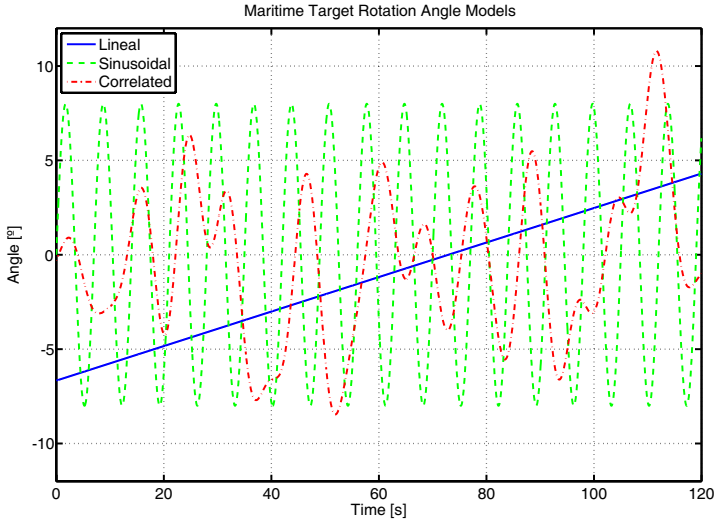

Figure 2. Example of rotation angles produced with the different models. The parameters for the linear model are $T_i = 350\,\mathrm{s}$ and for the sinusoidal and correlated model $\theta_{i_M} = \theta_{i_D} = 8.00°$, $T_i = 7\,\mathrm{s}$. The initial angles and phases are randomly selected.

frequency domain with a low pass correlation filter $H_{T_i}(\omega)$. This filter can be obtained from any low pass filter $H(\omega)$ scaling the frequency coefficients in order to preserve the unit variance of the signal. The correlation period T will be the inverse of the filter bandwidth. Finally the filtered signal is scaled with the desired deviation, θ_{i_D}.

$$\theta_i = \theta_{i_0} + \frac{2\pi}{T_i} \cdot t \tag{8}$$

$$\theta_i = \theta_{i_0} + \theta_{i_M} \cdot \sin\left(\frac{2\pi}{T_i} \cdot t + \phi_{i_0}\right) \tag{9}$$

$$\theta_i = \theta_{i_0} + \theta_{i_D} \cdot \mathcal{F}^{-1}\left\{H_{T_i}(\omega) \cdot W_i(\omega)\right\} \tag{10}$$

An example of rotations generated with each model can be shown in Figure 2. With the third model, more general and realistic combination of rotations are obtained, and is the model we will use in our simulations.

2.3. Target Model

To simulate a realistic echo return it is important to use a realistic model for the scattering location and strength. In order to accomplish

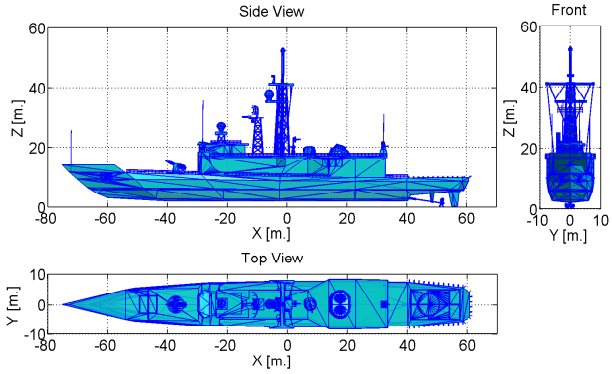

Figure 3. Three dimensional tessellation target model.

that, we employ a Standard Tessellation Language (STL) model as an input to the simulator. This 3-D model allow us to define both position and material properties that we use to specify the Radar Cross Section (RCS). The initial model used for the simulations, obtained from [18], can be seen in Figure 3.

In order to simulate echoes for high signal bandwidths it is often necessary to reduce the patch size. This is done by re-triangulating the surfaces of the initial tessellation until all of them are below the required size. With this approach we can simulate extended targets as a group of point targets controlling the accuracy just by configuring the patch size. If the patch size is small enough to have several point targets inside the radar resolution cell, phenomenons like speckle noise and phase scintillation are also taken into account [19].

2.4. Signal Model

The received echo signal is calculated using a Shooting and Bouncing Ray (SBR) technique [20, 21] and adding the contribution of each triangular facet of the target model. The return of these facets is modelled as a point scatter located at the barycentre position, according to the method presented in [22]. Shadowing that each facet cause in the others is taken into account and only direct contribution of the facets is considered.

In order to obtain interferometric images, we have to simulate the received signal in two phase centres associated to the receiving antennas. We will consider the antennas to be vertically displaced a distance B, called baseline, and centred respect to the radar position O. In addition, we assume the radar has an additional transmitting

antenna located at O. This geometry corresponds to the bi-static radar presented in [12]. For that kind of radar configuration, the interferometric height is obtained using the interferometric phase, which depends on the distance difference from the target to the lower receiving antenna r_L and with the upper receiving antenna r_U, as shown in (11). The height ambiguity is given by (12) for vertically displaced antennas.

$$\phi_I = \phi_L - \phi_U = -\frac{2\pi}{\lambda}(r_L - r_U) \tag{11}$$

$$h_a = \frac{\lambda \cdot r_L}{B} \tag{12}$$

3. INISAR SIGNAL PROCESSING

The first step in the InISAR signal processing chain is to generate an ISAR image for each of the receiving antennas. Then, those images are combined in order to obtain an interferogram which will be used to retrieve the interferometric phase. The last step is to convert the interferometric phase into height to form a representative InISAR image.

In order to generate the ISAR images for both receiving antennas we use the Global Range Alignment (GRA) described in [6] for translational movement compensation and the Polar Format Algorithm (PFA) described in [23, 24] for image formation. For the scope of this paper we are not concerned about focusing issues, so we assume that we know the targets dynamics in the PFA algorithm avoiding to use any particular autofocus algorithm. However, defocusing may still occur due to 3-D target movement mapping into the 2-D image plane selected. In the PFA an arbitrary image plane can be selected. We will only use the plane generated by the LOS direction and the elevation rotation vector. We call this plane the Vertical Plane which is the plane of interest in order to obtain a side-view of the target. The Doppler axis will be denoted by Vertical-Cross-LOS after the dimension scaling done in the PFA.

The wrapped interferometric phase, $\varphi_I(r, d)$, is obtained from the individual ISAR images, $ISAR(r, d)$, as shown by (13). However in order to obtain a correct height measurement we need the absolute interferometric phase, $\phi_I(r, d)$. The absolute phase difference can be obtained by phase unwrapping [25, 26]. However traditional phase unwrapping algorithms that assume a continous phase surface are not directly applicable to InISAR images [12]. Another option is to use an unambiguous extra interferometric pair for the distance of

interest, [11, 27], in order to obtain the correct phase cycle $n(r,d)$ in (14).

$$\varphi_I(r,d) = \arg\{ISAR_L(r,d) \cdot ISAR_U^*(r,d)\} \tag{13}$$

$$\phi_I(r,d) = \varphi_I(r,d) + 2\pi \cdot n(r,d) \tag{14}$$

However, in maritime surveillance applications, the distance between target and radar will be far enough to guarantee no ambiguity in target height measurement. As we can check with (12). Moreover, we know that the target will be placed in the sea surface and, of course, we can obtain its distance with the radar. So, the absolute phase and height above the surface can be derived because we know the general geometry. In order to make the measured height to represent the height above the surface it is necessary to remove the "flat-earth" phase term, $\varphi_{FE}(r)$, [19]. This term is the phase change related to the range difference between the receiving antennas and the sea surface for each range cell.

$$\phi_I(r,d) = \varphi_I(r,d) - \varphi_{FE}(r) \tag{15}$$

Interferometric phase will only present useful information in high coherence areas between both ISAR images. Areas with noise or affected by phase scintillation will present low coherence and will complicate height image interpretation. In order to generate a useful InISAR image all low coherence areas have to be removed from the image. The coherence operator, presented in (16), is used to generate the coherence image mask. However, low power areas, such as secondary lobes from prominent scatters, may have a high coherence but are of little interest for image interpretation. In order to remove those effects, a threshold in the image power $P(r,d)$ is combined with the threshold in the coherence map to form final image mask, $M(r,d)$. Only image pixels exceeding the coherence threshold, C_{th} and the power threshold, P_{th}, will form the final InISAR image, (18). The different images and the process of creating the InISAR image is illustrated in Figure 4.

$$C(r,d) = \frac{\langle ISAR_L(r,d) \cdot ISAR_U^*(r,d) \rangle}{\sqrt{\left\langle |ISAR_L(r,d)|^2 \right\rangle \cdot \left\langle |ISAR_U(r,d)|^2 \right\rangle}} \tag{16}$$

$$P(r,d) = |ISAR_L(r,d) \cdot ISAR_U^*(r,d)|^2 \tag{17}$$

$$M(r,d) = C(r,d) > C_{th} \;\&\; P(r,d) > P_{th} \tag{18}$$

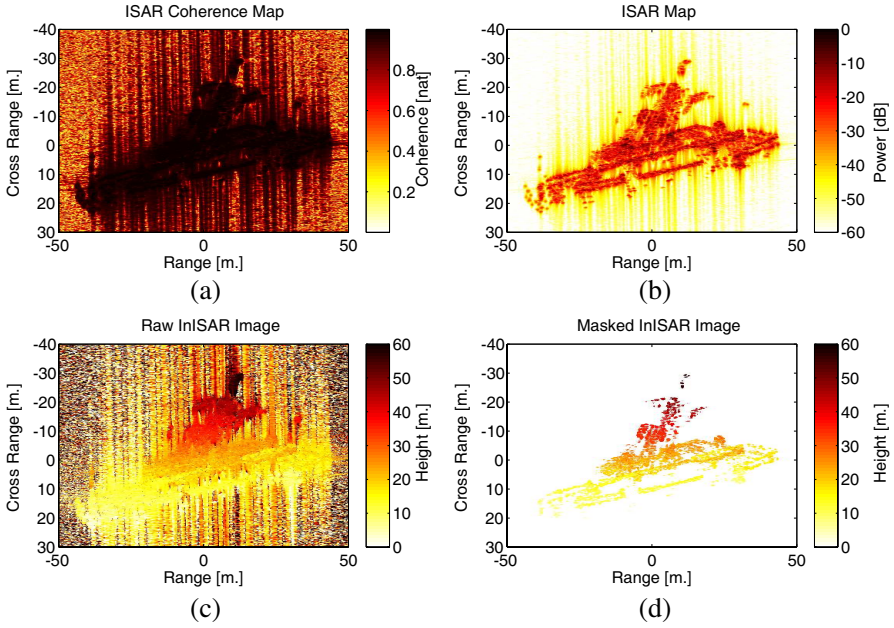

Figure 4. Coherence Map and InISAR final image formation. (a) Coherence between Isar Images. (b) Isar Power Map. (c) Raw InISAR image. (d) Power and Coherence mask applied to InISAR image.

4. DYNAMICS INFLUENCE AND UTILITY OF INISAR IMAGES

Targets roll, pitch and yaw rotations can be jointly represented by a rotation vector. The projection of this vector into a plane perpendicular to LOS is called the effective rotation vector [28]. ISAR image projection plane is defined as a plane that the effective rotation vector is normal to, and the LOS unit vector lies in [28]. The effective rotation vector will change with time so the image projection plane will be constantly changing.

In maritime applications we are typically interested in obtaining a side-view of the target in order to be able to identify and estimate the height of the masts, apart from measuring the total length. In those cases we will select a vertical imaging plane in the PFA assuming that height will be represented into the Doppler dimension. However, this is only true when the ship has a pitch dominant dynamics and is oriented exactly in the LOS direction. When a general composition of movements or an important deviation from LOS direction exist, the

imaging plane will no be aligned with the $\hat{x}-\hat{y}$ plane having a Doppler dimension that do not directly represent targets height. The same rational is applicable if we are interested in a top-view of the target and we use a horizontal imaging plane.

Using interferometry we can obtain the height of the target irrespective of the projection into the range-Doppler space. In order to verify it we have simulated a situation where a ship is moving away the radar with an orientation of 60° respect to LOS, a gracing angle of 5°, and general correlated rotations. The periods and maximum amplitude corresponds to a typical destroyer according to [10]. Attitude of the target is shown in Figure 5 where we have selected two imaging frames. In Frame I the target has a roll-dominated motion with little influence of pitch and yaw. On the other hand, Frame II has similar instantaneous angular rates in each axis.

In Frame I the target moves with a roll-dominant attitude but it has an important deviation with respect to LOS direction. However, it could be considerer as a good instant for ISAR imaging because the main Doppler gradient is caused by the different scatters height. So, if we know the target orientation, we can compensate for length and height projections. However, slight yaw rate will change the imaging plane making direct estimation of height more difficult. In the upper plot of Figure 6 we can see that the ISAR image obtained in this frame

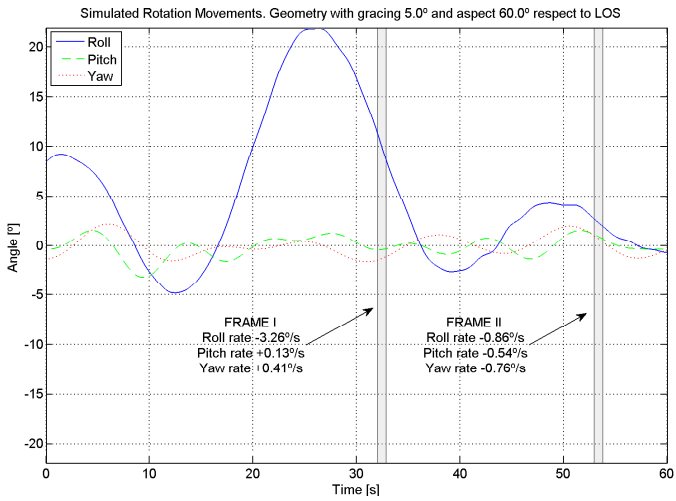

Figure 5. Simulated dynamics for a target orientated with 60° with respect to LOS. Mean roll period is 15 s, pitch 7 s and yaw 9 s. Standard roll deviation is 15°, pitch 2° and yaw 2°.

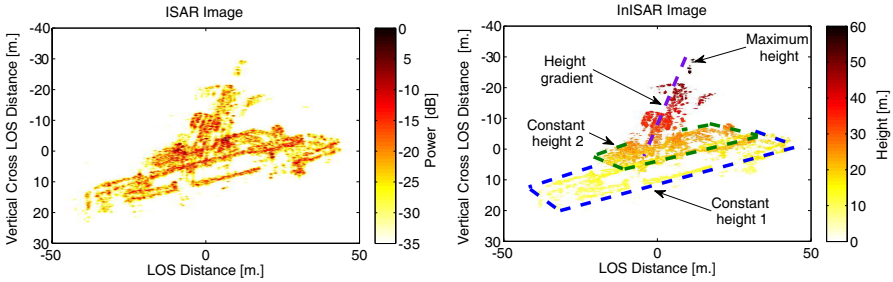

Figure 6. Simulated image in frame I. Aspect angle 60°, gracing angle 5°, roll rate −3.26°/s, pitch rate 0.13°/s, yaw rate 0.41°/s.

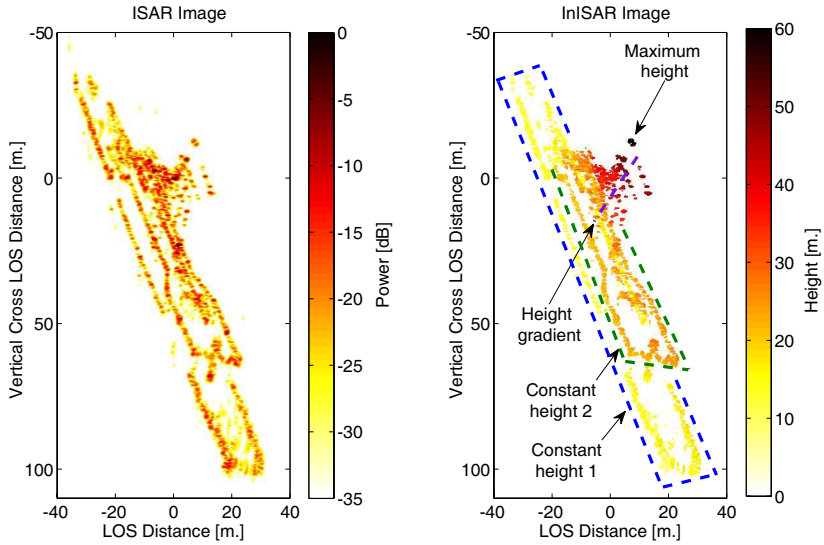

Figure 7. Simulated image in frame II. Aspect angle 60°, gracing angle 5°, roll rate −0.86°/s, pitch rate −0.54°/s, yaw rate −0.76°/s.

is nearly a side-view of the target. However, the Doppler dimension does not really represent the actual height. On the contrary, in the right plot of Figure 6, the InISAR image clearly shows the constant height surfaces of the target, the maximum height and the height gradient related to the masts. Moreover, these values are the actual height values with no need of compensation due to target orientation. It can be checked that InISAR image heights are in line with the model shown in Figure 3.

In Frame II the target has angular rates in every axis so the

projection in the image plane will be very complex. In the left plot of Figure 7 we can see that the ISAR image does not represent a side view and it is difficult to identify the masts or its heights. On the contrary, in the lower plot of Figure 7, we can clearly see in the InISAR image the maximum height of the target that will be associated to the principal mast. In addition, as in frame I, we can also identify the constant height and the height gradients.

With the images obtained in frame I and II we have seen how InISAR images can help to identify target features. However, under some circumstances the InISAR image can also be essential for ISAR image interpretation. Let us consider a much more unfavourable geometry for ISAR imaging. Figure 8 shows very similar dynamics to that presented in Figure 5 but the target is now orientated in the Cross-LOS direction. Selected imaging frames are Frame III and Frame IV.

Both figures obtained in frames III and frame IV are a mixture between a front-view and a top-view of the target. This makes ISAR image interpretation difficult. Left plot in Figure 9 shows a predominant front view of the target. However the image is quite blurred and it is very difficult to ensure without previous knowledge if it is a front or a top view. In Frame IV pitch gradient is higher

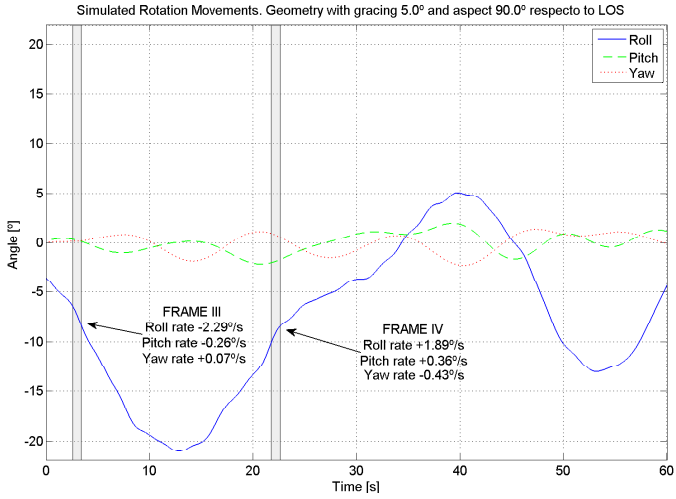

Figure 8. Simulated dynamics for a target aligned with the XLOS direction. Mean roll period is 15 s, pitch 7 s and yaw 9 s. Standard roll deviation is 15°, pitch 2° and yaw 2°.

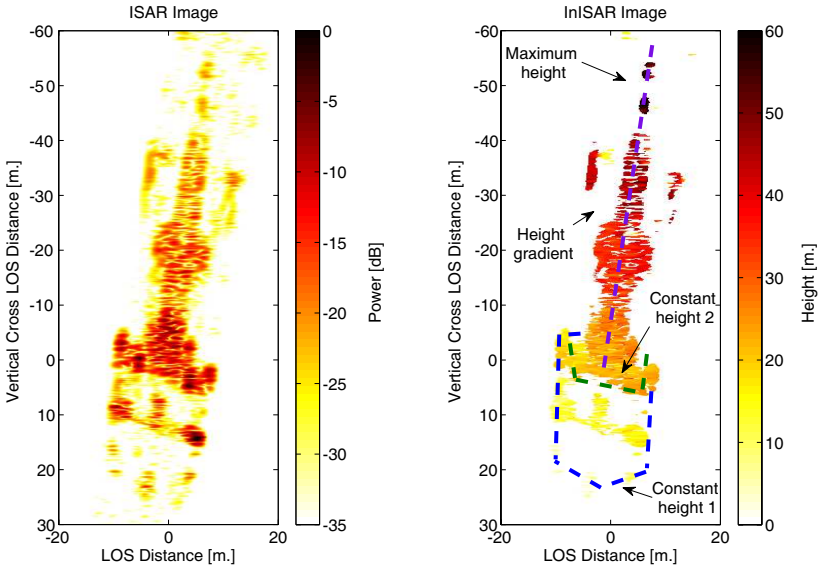

Figure 9. Simulated image in frame III. Aspect angle 90°, gracing angle 5°, roll rate −2.29°/s, pitch rate −0.26°/s, yaw rate 0.07°/s.

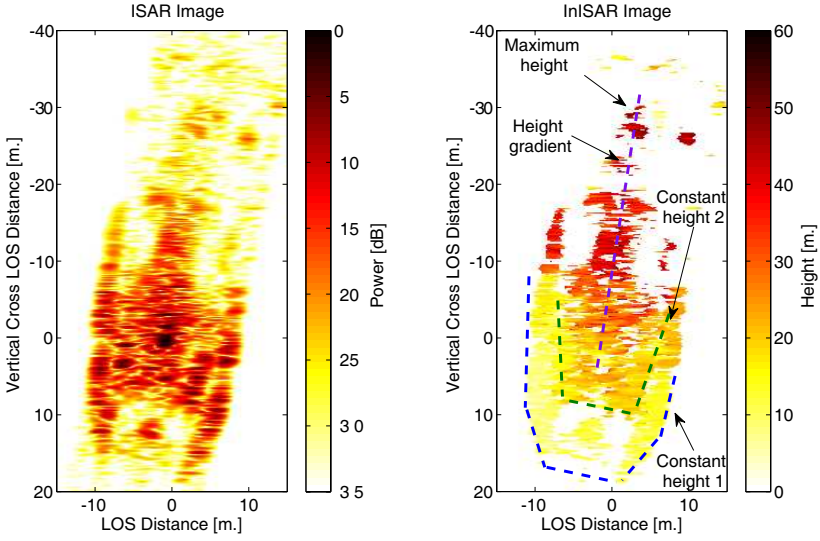

Figure 10. Simulated image in frame IV. Aspect angle 90°, gracing angle 5°, roll rate 1.89°/s, pitch rate 0.36°/s, yaw rate −0.43°/s.

than in frame III making top-view more present in the ISAR image, left plot in Figure 10, making interpretation really difficult even for trained operators.

With the help of the InISAR image, right plots in Figures 9 and 10, the operator can guess the position of the imaged target by identifying the constant height surfaces and the position of the height gradient in the image. This information would have been impossible to obtain just with the plain ISAR image.

5. CONCLUSIONS

In this paper we have shown the utility of using ISAR interferometry in maritime surveillance applications. InISAR images can aid target classification, by providing reliable height measurements, and also aid ISAR image interpretation in complicated geometries. In addition, we have described the simulator along with the models used in order to simulate realistic targets and dynamics. Several simulated images, in difficult geometries, has been presented to illustrate interferometric images utility and also showing the high quality and realistic images obtained with the described simulator.

ACKNOWLEDGMENT

This work has been supported by the projects TEC2008-02148/TEC and TEC2011-28683-C02-01 of the Spanish National Board of Scientific and Technology Research.

REFERENCES

1. Wehner, D. R., *High Resolution Radar*, 484, Artech House, Inc., Norwood, MA, 1987.
2. Xu, X. and R. M. Narayanan, "Three-dimensional interferometric ISAR imaging for target scattering diagnosis and modeling," *IEEE Transactions on Image Processing*, Vol. 10, No. 7, 1094–2003, 2001.
3. Ender, J. and A. Brenner, "PAMIR — A wideband phased array SAR/MTI system," *Radar, Sonar Navigation, IET*, Vol. 150, No. 3, 165–172, 2003.
4. Zhang, Y., W. Zhai, X. Zhang, X. Shi, X. Gu, and Y. Deng, "Ground moving train imaging by ku-band radar with two receiving channels," *Progress In Electromagnetics Research*, Vol. 130, 493–512, 2012.

5. Essen, H., M. Hagelen, A. Wahlen, K. Schulz, K. Jager, and M. Hebel, "ISAR imaging of helicopters using millimeter wave radars," *International Journal of Microwave and Wireless Technologies*, Vol. 1, No. 3, 171–178, 2009.
6. Wang, J. and D. Kasilinga, "Global range alignment for ISAR," *IEEE Transactions on Aerospace and Electronic Systems*, Vol. 39, No. 1, 351–357, 2003.
7. Ender, J., L. Leushacke, A. Brenner, and H. Wilden, "Radar techniques for space situational awareness," *Radar Symposium (IRS), 2011 Proceedings International*, 21–26, Sept. 2011.
8. Munoz-Ferreras, J. M. and F. Perez-Martinez, "Pitch estimation for non-cooperative maritime targets in ISAR scenarios," *Radar, Sonar Navigation, IET*, Vol. 3, No. 5, 521–529, 2009.
9. Martorella, M., "Novel approach for ISAR image cross-range scaling," *IEEE Transactions on Aerospace and Electronic Systems*, Vol. 44, No. 1, 281–294, 2008.
10. Doerry, A. W., "Ship dynamics for maritime ISAR imaging," Report SAND2008-1020, 32, Sandia National Laboratories, 2008.
11. Ma, C.-Z., T. S. Yeo, H. S. Tan, and G. Lu, "Interferometric isar imaging on squint model," *Progress In Electromagnetics Research Letters*, Vol. 2, 125–133, 2008.
12. Felguera-Martín, D., J.-T. González-Partida, P. Almorox-González, M. Burgos-García, and B.-P. Dorta-Naranjo, "Interferometric inverse synthetic aperture radar experiment using an interferometric linear frequency modulated continuous wave millimetre-wave radar," *Radar, Sonar Navigation, IET*, Vol. 5, No. 1, 39–47, 2011.
13. Wu, B.-I., M. C. Yeuing, Y. Hara, and J. A. Kong, "Insar height inversion by using 3-D phase projection with multiple baselines," *Progress In Electromagnetics Research*, Vol. 91, 173–193, 2009
14. Park, J.-I. and K.-T. Kim, "A comparative study on ISAR imaging algorithms for radar target identification," *Progress In Electromagnetics Research*, Vol. 108, 155–175, 2010.
15. Li, H. J. and V. Chiou, "Aerospace target identification-comparison between the matching score approach and the neural network approach," *Journal of Electromagnetic Waves and Applications*, Vol. 7, No. 6, 873–893, 1993.
16. Li, H. J. and K. M. Li, "Application of wavelet transform in target identification," *Progress In Electromagnetics Research*, Vol. 12, 57–73, 1996.
17. Seo, D.-K., K.-T. Kim, I.-S. Choi, and H.-T. Kim, "Wide-

angle radar target recognition with subclass concept," *Progress In Electromagnetics Research*, Vol. 44, 231–248, 2004.

18. http://sketchup.google.com/3dwarehouse/details?mid=405772569eb4f248c1ccec171a275967&prevstart=0
19. Rosen, P. A., S. Hensley, I. R. Joughin, F. K. Li, S. N. Madsen, E. Rodriguez, and R. M. Goldstein, "Synthetic aperture radar interferometry," *Proceedings of the IEEE*, Vol. 88, No. 3, 333–382, 2000.
20. He, X.-Y., X.-B. Wang, X. Zhou, B. Zhao, and T.-J. Cui, "Fast isar image simulation of targets at arbitrary aspect angles using a novel sbr method," *Progress In Electromagnetics Research B*, Vol. 28, 129–142, 2011.
21. Bhalla, R. and H. Ling, "ISAR image formation using bistatic computed from shooting and bouncing ray technique," *Journal of Electromagnetic Waves and Applications*, Vol. 7, No. 9, 1271–1287, 1993.
22. García-Fernández, A. F., O. A. Yeste-Ojeda, and J. Grajal, "Facet model of moving targets for ISAR imaging and radar back-scattering simulation," *IEEE Transactions on Aerospace and Electronic Systems*, Vol. 46, No. 3, 1455–1467, 2010.
23. Carrara, W. G. and R. S. Goodman, *Spotlight Synthetic Aperture Radar, Signal Processing Algorithms*, Artech House, Inc., 1995.
24. Mao, X., D.-Y. Zhu, and Z.-D. Zhu, "Signatures of moving target in polar format spotlight SAR image," *Progress In Electromagnetics Research*, Vol. 92, 47–64, 2009.
25. Ren, X.-Z., Y. Qin, and L. H. Qiao, "Interferometric properties and processing for spaceborne spotlight SAR," *Progress In Electromagnetics Research B*, Vol. 36, 267–281, 2012.
26. Li, C. and D.-Y. Zhu, "A residue-pairing algorithm for insar phase unwrapping," *Progress In Electromagnetics Research*, Vol. 95, 341–354, 2009.
27. Liu, C., X. Gao, W. Jiang, and X. Li, "Interferometric isar three-dimensional imaging using one antenna," *Progress In Electromagnetics Research M*, Vol. 21, 33–45, 2011.
28. Chen, V. C. and W. J. Miceli, "Simulation of ISAR imaging of moving targets," *IEE Proceedings on Radar, Sonar and Navigation*, Vol. 148, No. 3, 160–166, 2001.